3-D Finite Element Analysis of Long-Fiber Reinforced Composite Spur Gears

Çağdaş Alagöz, M.A. Sahir Arikan, Ö. Gündüz Bilir and Levend Parnas

This article was originally presented at the 2000 ASME Design Engineering Technical Conferences, held in Baltimore, MD, in September 2000. Reprinted with *permission.*

This article describes a method and a computer program that were developed for 3-D finite element analysis of long-fiber reinforced composite spur gears, in which long fibers are arranged along tooth profiles. For such a structure, the gear is composed of two regions; namely the long-fiber reinforced and the chopped-fiber reinforced regions.

Introduction

Compared with monolithic materials, composites have unique advantages, such as high strength, high stiffness, long fatigue life, low density, and adaptability to the function of the structure. Additional improvements can be realized in the corrosion resistance, wear resistance, appearance, temperature-dependent behavior, thermal stability, thermal insulation, thermal conductivity and acoustic insulation.

Plastic gears have excellent properties, such as self-lubrication, high chemical resistance, low noise and high impact resistance, but they are inferior to steel gears in their load capacities. For this reason, there are few examples of plastic gears being used for power transmission. If plastic gears reinforced with high-strength fibers, such as glass or carbon fibers, are realized, they will become useful plastic gears of high strength, as well as having the above-mentioned properties.

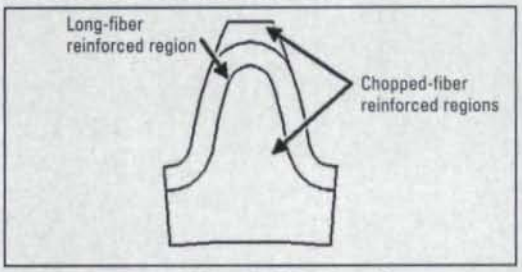

Figure 1—Long-fiber reinforced tooth.

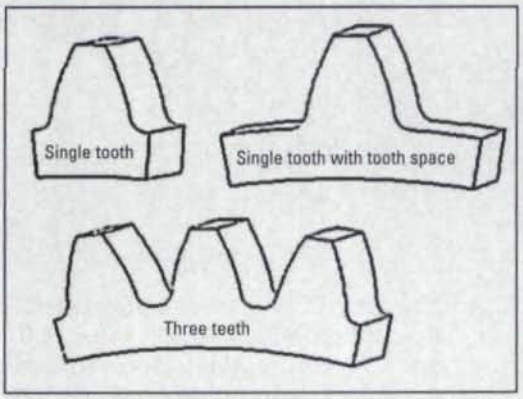

Figure 2—Gear models that can be generated by the developed program.

Although it is relatively easy to manufacture composite gears reinforced with chopped or particulate fibers by using the method used for isotropic gears, manufacturing a composite gear filled with long fibers is technically difficult. There are studies both on composite gears manufactured from chopped- or particulate-fiber reinforced materials (Refs. 11 and 9), and on long-fiber reinforced composite gears (Ref. 8). Almost no attempt has been made to investigate the possible stress and deformation variations for gears that could have been made of an orthotropic material.

In this study, composite spur gears, in which long fibers are arranged along tooth profiles, are analyzed in 3-D by using the finite element analysis method (Ref. 2). This type of composite spur gear was manufactured by Shiratori et al. (Ref. 8). A casting method was adopted to manufacture the gears. As shown in Figure 1, for such a structure, the gear is composed of two regions, which are the long-fiber reinforced and the chopped-fiber reinforced regions. It is important to note that there is almost no approach to analyze this type of composite gear because of different fiber orientations at different sections of the long-fiber reinforced region of the tooth.

Since elements have different orientations and material properties, for the finite element analysis of this type of composite gear with complex geometries, material properties of each element constituting the mesh should be defined separately. Forming the model geometry, subdividing it into elements, finding the appropriate mesh density and preparing the input data for a finite element

program becomes a complex and time-consuming task, which is impossible to perform manually. All of the above-mentioned tasks are performed by the pre-processing module of the developed program. Main inputs for this module of the program are information on basic gear geometry, gear drive data, material properties and long-fiber reinforcement geometry. Finite element meshes are automatically generated, and mesh information with other required data is written to a file in the input-file format of ABAQUS®. Stresses are read from the output file of ABAQUS® by the post-processing module, and color-coded drawings for various stresses and failure indexes are displayed. For the long-fiber reinforced region, failure indexes are calculated by using the tensor polynomial failure criterion used by Herakovich (Ref. 5).

Finite Element Modeling

Finite element modeling mainly consists of gear model selection, mesh generation, boundary condition input, material definition and load definition. The first step is the selection of the gear model among the ones given in Figure 2. Next, the tooth profile is divided into segments, and the mesh is automatically generated for long-fiber reinforced and chopped-fiber reinforced regions. First, a 2-D mesh is generated. Then, the 3-D mesh is formed by considering the face width of the gear and the number of divisions specified in this direction. During mesh generation, thicknesses and locations of fiber arrangements and mesh density can be controlled. Then, boundary conditions, material definition and load definition are entered. Finally, mesh information and other required data are written to a file in the input-file format of ABAQUS®.

Gear Models. In the literature, various models are used for finite element analysis of gears. These include single-tooth models, models with one full tooth and two partial teeth at both sides, models with one full tooth and the tooth spaces on both sides, and three-tooth models. The most suitable model is determined by comparing the stresses found by using different models. Since all the models were developed and used for isotropic materials, the same comparisons should be made for composite materials. The program by the authors is capable of generating meshes by using the gear models given in Figure 2.

Generation of the Outside Profile for the Model. As shown in Figure 3, the outside profile of the model is generated by using seven guide points. Point 1 is on the tooth centerline; point 2 is at the tooth tip. The segment between points 2 and 3 is the involute tooth profile; the segment

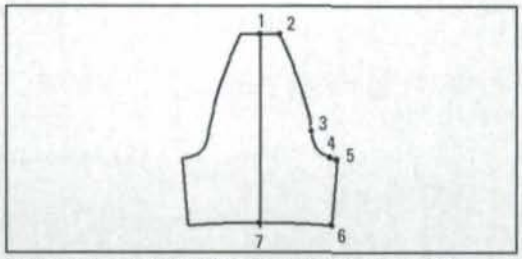

Figure 3—Guide points on the outside profile.

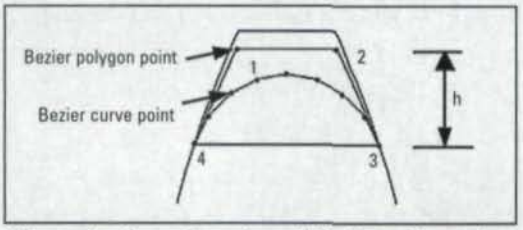

Figure 4—Upper boundary of the long-fiber reinforced region formed by using a bezier curve.

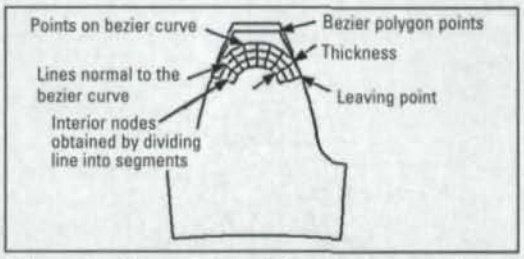

Figure 5—Generated mesh for the upper section of the long-fiber reinforced region.

bounded by points 3 and 4 is the trochoid tooth fillet profile. Point 5 is on tooth space centerline. The rim thickness of the gear is the distance between points 5 and 6. Finally, point 7 is again on the tooth centerline. Calculations on gear geometry and tooth profiles are made using the methods and equations of Arikan (Refs. 3–4).

Mesh Generation for the Long-Fiber Reinforced Region. In the long-fiber reinforced region, fibers are inserted into the tooth along the tooth profile. Bezier curves are used to form the geometry of the fibers. The shape of a Bezier curve can be controlled by making use of a defining polygon. As shown in Figure 4, four points are sufficient to form the polygon and the Bezier curve.

During mesh generation, lines normal to the Bezier curve and passing through the Bezier points are drawn. Line lengths are made equal to the fiber thickness. Interior nodes are obtained by dividing the lines into segments, as shown in Figure 5.

As seen in Figure 5, above the leaving point, fibers are not parallel to the tooth profile, but have a curved shape determined by the Bezier curve geometry. Below the leaving point, fibers become parallel to the tooth profile. Interior nodes below the leaving point can be generated by moving into the tooth in a direction normal to

Çağdaş Alagöz
worked on this subject as part of his master of science program at Middle East Technical University, located in Ankara, Turkey.

Dr. M.A. Sahir Arikan
is a professor in the department of mechanical engineering at Middle East Technical University. His areas of interest include CAD/CAM, robotics, machine elements, machine design, gear design and gear dynamics.

Dr. Ömer Gündüz Bilir
is a professor in the department of mechanical engineering at Middle East Technical University. His areas of interest include experimental stress analysis, fracture mechanics and composite materials.

Dr. Levend Parnas
is an associate professor and assistant chairperson of the department of mechanical engineering at Middle East Technical University. His areas of interest include composite structures, computational analysis of structures, fracture mechanics, experimental mechanics and biomechanics.

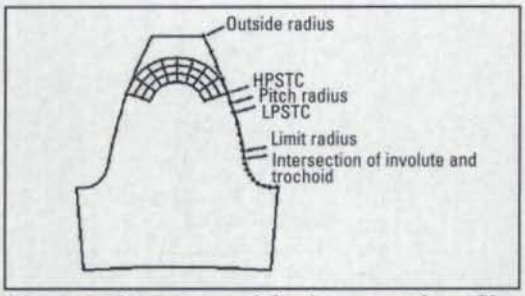

Figure 6—Nodes at special points on tooth profile.

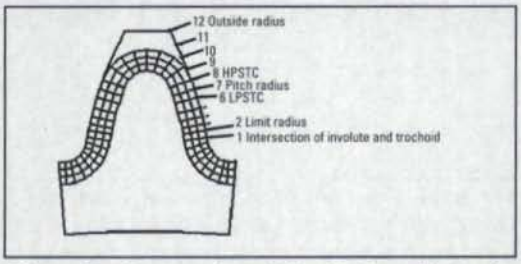

Figure 7—Generated mesh for the long-fiber reinforced region.

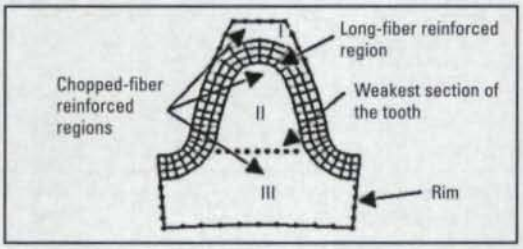

Figure 8—Sub-regions of the chopped-fiber reinforced region.

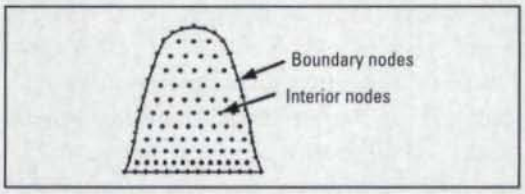

Figure 9—Boundary and interior nodes of sub-region II.

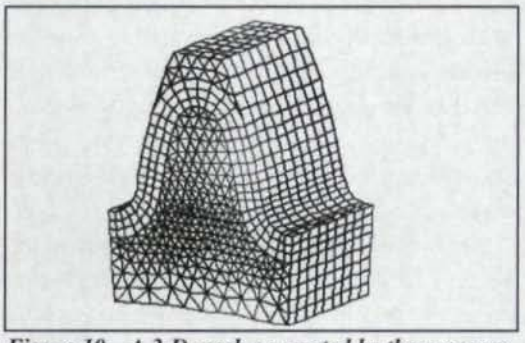

Figure 10—A 3-D mesh generated by the program.

the tooth profile. For this purpose, the first step is allocation of the nodes on the tooth profile. Since a finite element model can only be loaded at the nodes, first, nodes are allocated at special points for which solutions are desired; then intermediate nodes are formed between the special nodes. These special points are: highest point of contact (HPC), corresponding to outside radius; highest point of single tooth contact (HPSTC); pitch point, corresponding to pitch radius; lowest point of single tooth contact (LPSTC); lowest point of contact (LPC), corresponding to limit radius; and the point corresponding to the radius at which the involute tooth profile joins the trochoid fillet profile. Nodes allocated at the special points are given in Figure 6. Figure 7 shows the generated mesh for the long-fiber reinforced region.

Mesh Generation for the Chopped-Fiber Reinforced Region. A two-dimensional automatic triangular mesh generation algorithm (Refs. 6 and 12) is used for generation of the mesh for the chopped-fiber reinforced region. In order to be able to control the mesh density and have larger densities at critical areas, the region is separated into three sub-regions, as shown in Figure 8.

Mesh generation is performed in four steps: allocation of the nodes at the boundaries, generation of the interior nodes, formation of triangular elements, and smoothing of the mesh after triangulation.

Nodes at the boundaries are allocated by using the specified number of divisions for the sub-regions. For a sub-region, the boundary is represented by a disjoint union of a simple closed loop of straight-line segments. Then, the interior nodes are allocated by using the specified number of divisions. Figure 9 shows the boundary and interior nodes allocated in sub-region II.

Next, all of the nodes are connected, and triangular elements are formed in such a way that there are no overlapping elements and the entire region is covered. The triangulation scheme is designed to produce elements as near to equilateral triangles as the system of nodal points permits (Ref. 6). After triangulation, in order to have more equal element sizes, the smoothing process follows. Usually, the process converges after two cycles. Finally, elements in the tooth width direction are generated by considering the face width of the gear and the number of divisions specified in this direction. A 3-D mesh generated by the program can be seen in Figure 10. Sample 2-D meshes generated for different fiber arrangements and with different mesh resolutions are given in Figure 11.

Boundary Conditions, Material Definition and Load Definition. Two different boundary conditions can be used for the analysis. For solid gears, as shown in Figure 12a, all of the nodes at the sides and bottom of the model are fixed. For thin-rim gears, as given in Figure 12b, only the nodes at the sides are fixed. When material properties are considered, as mentioned before, two regions with different properties exist within the

gear. These regions are the long-fiber reinforced region, in which unidirectional fibers are present, and the chopped-fiber reinforced region, in which there are randomly oriented, discontinuous fibers. If the fiber orientation in a composite material is truly random in a three-dimensional sense, the composite exhibits three-dimensional isotropy. Therefore, the material forming the chopped-fiber reinforced region can be considered as a material with a single elastic modulus and Poisson's ratio. In the long-fiber reinforced region, as shown in Figure 13, each element is a unidirectional, fiber-reinforced composite and has different material properties with respect to the global coordinate system because of its orientation. On the other hand, elements have the same elastic properties in the local coordinate system given in Figure 14. The local coordinate system is obtained by rotating the global coordinate system about axis 3 by the required angle. As seen in Figure 15, all of the elements in a slice have the same orientation and consequently the same elastic properties with respect to the global coordinate system. Thus, all elements in a slice can be reduced to an element set. Elastic properties of element sets are defined in their local coordinate systems.

For loading, distributed loads in the tooth width direction are resolved as shown in Figure 16. Thus, a uniform displacement distribution is obtained in the face-width direction (Ref. 3). Loads are applied to the nodes in a direction normal to the tooth profile.

Post-Processing of Results

For failure analysis, stresses are read from the output file of ABAQUS®, and color-coded drawings for various stresses and failure indexes are displayed. Figure 17 shows a sample output screen for failure index. Numerical values of the stresses and the failure index for an element can be displayed by bringing the cursor on the element and clicking the mouse button. In the figure, the black-colored element is the one for which the numerical results are displayed. At this step, it is also possible to replace the previously input material properties with new ones, and see new failure index values.

A tensor polynomial failure criterion (Ref. 5) is used to calculate the failure index for the long-fiber reinforced region. According to this criterion, failure occurs when,

$$f(\sigma_{ij}) = F_1\sigma_1 + F_2\sigma_2 + F_3\sigma_3 + F_{11}\sigma_1^2 + F_{22}\sigma_2^2 + F_{33}\sigma_3^2 + F_{44}\sigma_4^2 + F_{55}\sigma_5^2 + F_{66}\sigma_6^2 + 2F_{12}\sigma_1\sigma_2 + 2F_{13}\sigma_1\sigma_3 + 2F_{23}\sigma_2\sigma_3 \geq 1 \quad (1)$$

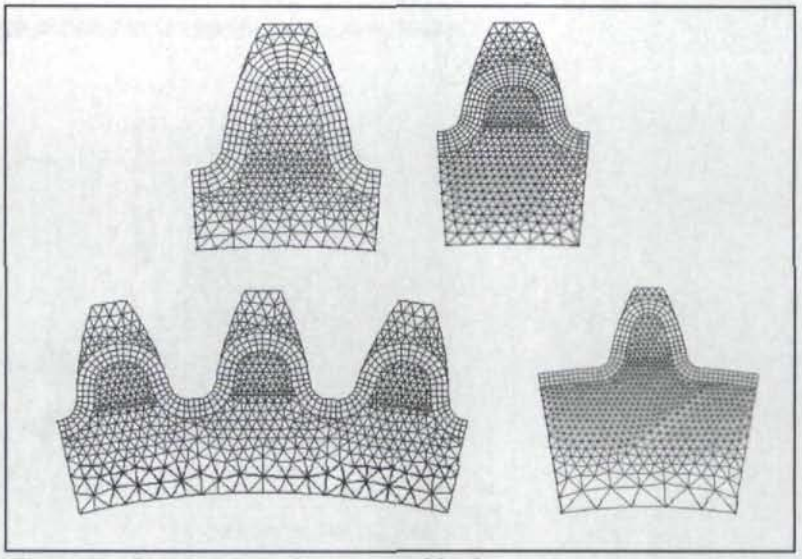

Figure 11—Sample 2-D meshes generated by the program.

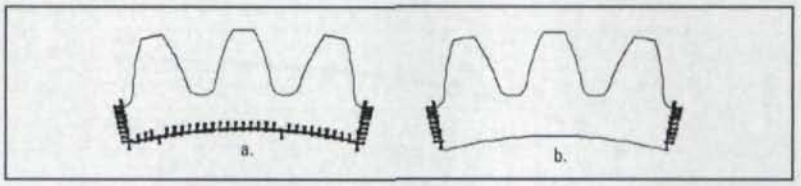

Figure 12—Boundary conditions.

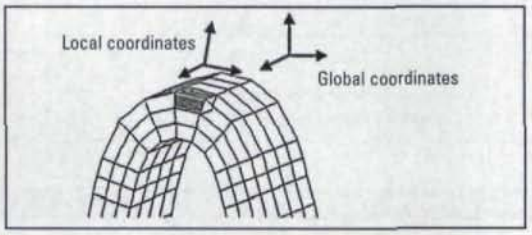

Figure 13—Fiber reinforcement in the long-fiber reinforced region.

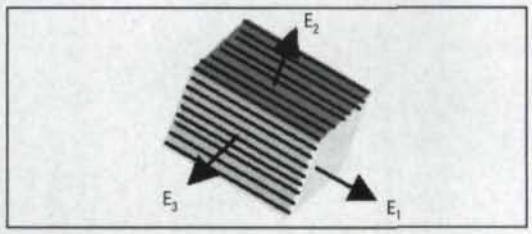

Figure 14—Material directions in the long-fiber reinforced region.

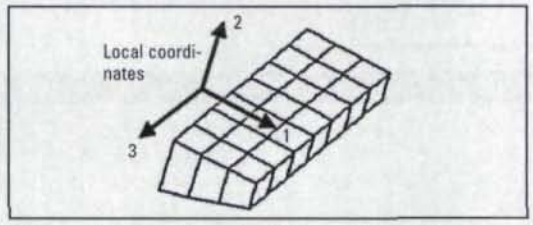

Figure 15—An element set formed by a slice.

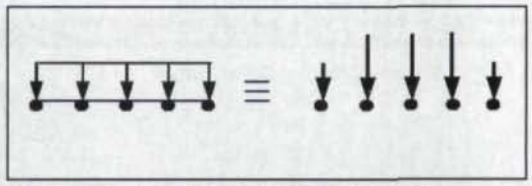

Figure 16—Resolution of distributed loads.

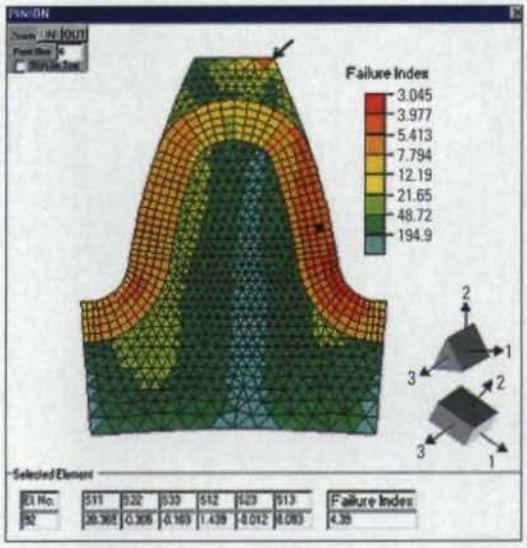

Figure 17—Sample output screen.

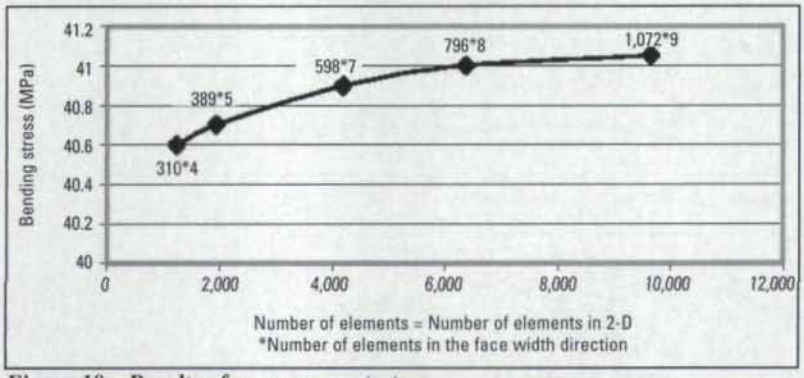

Figure 18—Results of convergence tests.

Table 1—Isotropic Spur Gear Data.

Basic Gear Geometry	
Pressure Angle	20°
Module, m	4.5 mm
Addendum	1.000 x m
Dedendum	1.250 x m
Generating Tool Tooth Tip Fillet Radius	0.300 x m
Gear	
Number of Teeth	72
Face Width	6.25 mm
Rim Thickness	2 x m
Material	
Elastic Modulus	210 GPa
Poisson's Ratio	0.3
Loading	
Load at Tooth Tip	500 N

Table 2—Bending Stresses at Tooth Root.

Tooth Model	Maximum Bending Stress (MPa)	
	Tensile	Compressive
Single Tooth	40.9	–48.2
Single Tooth with Tooth Space	39.7	–47.3
Three Teeth	39.8	–47.9

Table 3—Maximum Bending Stress at Tooth Root for Isotropic Gear.

Source	Maximum Bending Stress (MPa)
Developed Program	6.171
AGMA Equations	6.212
Oda et al. (FEM)	6.290
Oda et al. (Experimental)	6.236

where,

$$F_1 = \frac{1}{X_T} + \frac{1}{X_C}; \quad F_{11} = \frac{-1}{X_T X_C} \tag{2}$$

$$F_2 = \frac{1}{Y_T} + \frac{1}{Y_C}; \quad F_{22} = \frac{-1}{Y_T Y_C} \tag{3}$$

$$F_3 = \frac{1}{Z_T} + \frac{1}{Z_C}; \quad F_{33} = \frac{-1}{Z_T Z_C} \tag{4}$$

$$F_{44} = \frac{1}{Q^2}, \; F_{55} = \frac{1}{R^2}, \; F_{66} = \frac{1}{S^2} \tag{5}$$

In the above equations, X_T, X_C, Y_T, Y_C, Z_T and Z_C indicate tensile and compressive strengths in X, Y and Z directions; and Q, R and S indicate shear strengths in XY, XZ and YZ planes, respectively. Tsai and Hahn (Ref. 10) have proposed the following equations for interaction coefficients F_{12}, F_{13} and F_{23}.

$$F_{12} = -\frac{(F_{11} F_{22})^{1/2}}{2} \tag{6}$$

$$F_{13} = -\frac{(F_{11} F_{33})^{1/2}}{2} \tag{7}$$

$$F_{23} = -\frac{(F_{22} F_{33})^{1/2}}{2} \tag{8}$$

Failure index is defined as the inverse of $f(\sigma_{ij})$ given in Equation 1. Thus, a failure index less than one indicates failure, and a large failure index means a large margin of safety.

Verification of the Model

The model is verified by specifying all of the elements of the mesh as isotropic elements and comparing the results with previous results given for isotropic materials. Before the solution, convergence tests are performed, and a proper tooth model is determined. The spur gear with properties given in Table 1 is used for the tests. For the solution, all of the nodes at the sides and bottom of the model are fixed. Results of the covergence tests are given in Figure 18. By making use of the figure, it is decided to use about 6,000 elements (800 elements in 2-D and 8 divisions in the face width direction).

Bending stresses at the tooth root found by using different tooth models are given in Table 2. By making use of the table, it is decided to use the single-tooth model for the stress analysis, since more complex models give stresses that are only a few percent different than the ones given by the single-tooth model.

After deciding on the tooth model and the number of elements, tooth root stresses found for

isotropic gears by using the model are compared to the results found by using AGMA equations (Ref. 1) and results given by Oda et al. (Ref. 7). Stresses given in Table 3 are again for the gear whose properties are shown in Table 1. In order to be able to compare the stresses with the results given by Oda et al. (Ref. 7), instead of 500 N, a tip load of 1 kg_f /mm is applied to the tooth. It is found that stresses calculated using the model are in good agreement with other results.

Sample Results

Sample results are obtained for the composite spur gear whose properties are given in Table 4. In the long-fiber reinforced and chopped-fiber reinforced regions, glass/epoxy is used. Material properties of the long-fiber reinforced, unidirectional composite material are shown in Table 5, and material properties of the chopped-fiber reinforced composite are shown in Table 6 (Ref. 8).

As shown in Figure 19, from a failure point of view, there are three critical sections in a composite gear tooth. In section 1, the critical stress component is the axial tensile stress in the direction parallel to the fibers. During a failure in this section, fibers are broken. In sections 2 and 3, the critical stress component is the transverse tensile stress in the direction normal to the fibers. During failures in these sections, fiber separation is observed. Arrows at the ends of the lines marking the critical sections indicate the failure direction.

Results obtained by using the developed program for glass/epoxy and carbon/epoxy gears, together with the results given by Shiratori, et al. (Ref. 8) are shown in Figures 20 and 21, respectively. For failure analysis of isotropic materials, the maximum stress should be considered; for unidirectional materials, the stress along the fiber direction should be considered. Thus, for the chopped-fiber reinforced regions (inside of the tooth), the ratio of the stress (in the direction parallel with the tooth centerline) to the strength is calculated at the critical (weakest) section of the tooth. For the long-fiber reinforced region (the region next to the outside surface of the tooth), the ratio of the stress along the fiber direction to the strength in the same direction is calculated. As seen in the figures, results of the program agree well with the results given by Shiratori, et al. (Ref. 8).

Effects of reinforcing thickness of the long-fiber reinforced region and the insertion depth of the fibers on strengths of glass/epoxy gears are shown in Figures 22 and 23, respectively. During interpretation of the results, failure is always observed in section 2, where the critical stress component is the transverse tensile stress in the direction normal to the fibers. As seen in Figure 22, the failure index (and the strength) increases with increasing reinforcing thickness until the thickness becomes 1.5 mm. Beyond 1.5 mm, reinforcing thickness has no positive effect on gear strength.

Figure 22 shows the effect of insertion depth (h_f) of the fibers on gear strength. Increased insertion depth has a small positive effect on gear strength.

In order to see the effects of different materials and different fiber volume ratios for long-fiber

Table 4—Composite Spur Gear Data.

Basic Gear Geometry	
Pressure Angle	20°
Module, m	5 mm
Addendum	1.000 x m
Dedendum	1.250 x m
Generating Tool Tooth Tip Fillet Radius	0.300 x m
Gear	
Number of Teeth	30
Face Width	6.25 mm
Rim Thickness	2 x m
Material	
Elastic Modulus	210 GPa
Poisson's Ratio	0.3
Loading	
Loading at Tooth Tip	1 kg_f/mm

Table 5—Material Properties for the Long-Fiber Reinforced Region (Unidirectional Composite).

		Glass/Epoxy	Carbon/Epoxy
Axial Modulus, E_1	GPa	15.2	31.7
Transverse Modulus, E_2	GPa	6.53	5.63
Shear Modulus, G_{12}	GPa	1.71	1.7
Poisson's Ratio, υ_{12}		0.13	0.06
Poisson's Ratio, υ_{23}		0.08	0.03
Fiber Volume Ratio, V_f		0.3	0.3
Axial Tensile Strength	MPa	103	289
Axial Compressive Strength	MPa	261	326
Transverse Tensile Strength	MPa	28.2	11.0
Transverse Compressive Strength	MPa	588	334
Transverse Shear Strength	MPa	41.4	37.6

Table 6—Material Properties for the Chopped-Fiber Reinforced Region (Isotropic Composite).

		Glass/Epoxy	Carbon/Epoxy
Elastic Modulus, E_1	GPa	9.2	17
Poisson's Ratio, υ_{12}		0.31	0.33
Fiber Volume Ratio, V_f		0.2	0.2
Tensile Strength	MPa	36	48
Compressive Strength	MPa	116	116
Shear Strength	MPa	98	98
Transverse Shear Strength	MPa	41.4	37.6

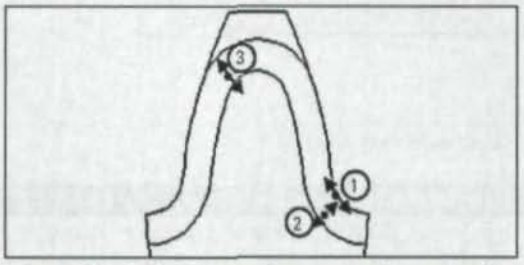

Figure 19—Critical sections in a composite gear tooth.

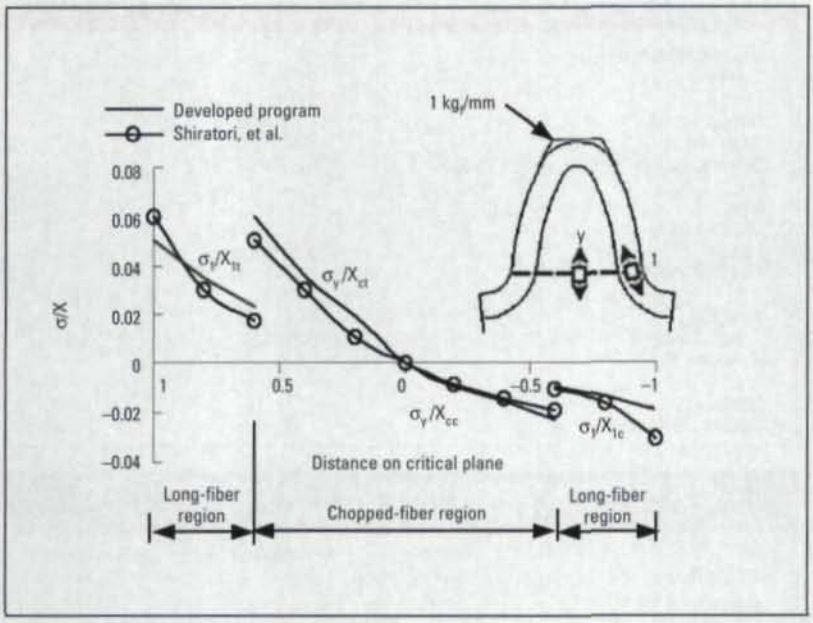

Figure 20—Stress Ratios for Glass/Epoxy Gear.

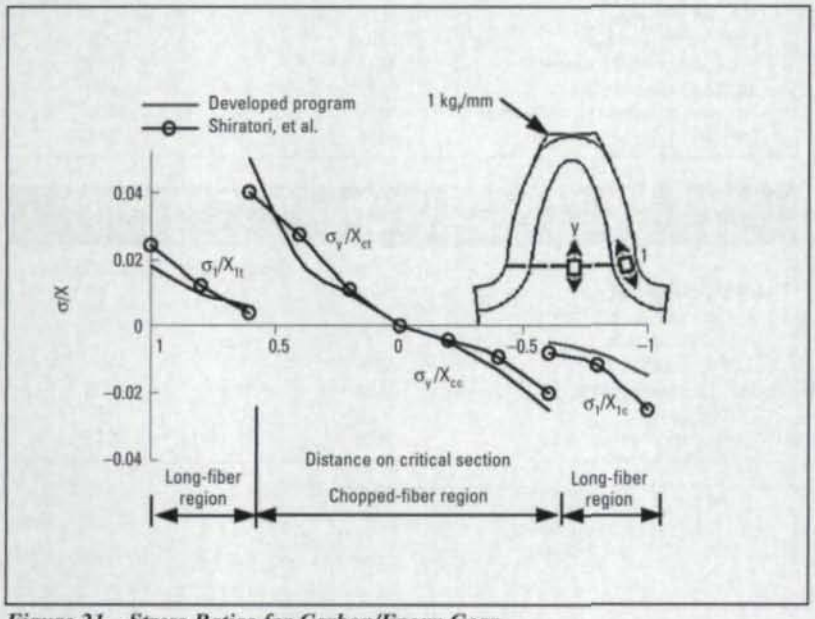

Figure 21—Stress Ratios for Carbon/Epoxy Gear.

Table 7—Material Properties for the Fibers.

		S-Glass	Carbon	Kevlar	Boron
Longitudinal Elastic Modulus	MPa	85,600	235,000	135,000	385,000
Transverse Elastic Modulus	MPa	85,600	16,550	5,200	385,000
Longitudinal Shear Modulus	MPa	5,170	14,400	2,890	166,500
Longitudinal Poisson's Ratio		0.22	0.2	0.35	0.21
Tensile Strength	MPa	4,200	2,599	3,445	3,900
Compressive Strength	MPa	520	2,500	551	4,550
Shear Strength	MPa	350	400	275	700

Table 8—Material Properties for the Matrix (Epoxy).

Elastic Modulus	MPa	4,200
Shear Modulus	MPa	1,340
Poisson's Ratio		0.38
Tensile Strength	MPa	52
Compressive Strength	MPa	130
Shear Strength	MPa	85

reinforced and chopped-fiber reinforced regions on gear strength, stress analyses are made for s-glass/epoxy, carbon/epoxy, kevlar/epoxy and boron/epoxy gears. For chopped-fiber reinforced regions, fiber volume ratios (V_{cf}) of 0.1, 0.3, 0.5 and 0.7 are used; for the long-fiber reinforced region, fiber volume ratios (V_{lf}) of 0.1, 0.3 and 0.5 are used. The same fiber and matrix materials are used for long-fiber reinforced and chopped-fiber reinforced regions.

Material properties for the fibers and the matrix are given in Tables 7 and 8, respectively. As a measure of the strength, calculated minimum failure index values together with the critical sections at which they are observed are given for s-glass/epoxy, carbon/epoxy, kevlar/epoxy and boron/epoxy gears in Tables 9–12.

Fiber volume ratio combinations, which result in the weakest and the strongest gears, are shown in Tables 13 and 14, respectively. As seen in the tables, for different materials, different fiber volume ratios should be used in order to obtain the strongest possible gear.

Discussion and Conclusion

A method and a computer program have been developed for 3-D finite element analysis of long-fiber reinforced composite spur gears, in which long fibers are arranged along tooth profiles. The developed program is verified by performing stress analysis on isotropic gears. Results of the program are compared to the results given for composite gears by Shiratori, et al. (Ref. 8), and good agreement is observed. Although the program is capable of using three different tooth models—namely single tooth, one full tooth with tooth spaces at both sides and three-tooth models—it is found that results given by the single-tooth model are satisfactory for stress analysis purposes.

For glass/epoxy gears, effects of reinforcing thickness of the long-fiber reinforced region and insertion depth of the fibers on gear strength are investigated. It is found that strength increases with increasing reinforcing thickness until a critical thickness is reached. Beyond the critical thickness, reinforcing thickness has no positive effect on gear strength. On the other hand, increased insertion depth has a small positive effect on gear strength.

Finally, in order to see the effects of different materials and different fiber volume ratios for long-fiber reinforced and chopped-fiber reinforced regions on gear strength, stress analyses are made for s-glass/epoxy, carbon/epoxy, kevlar/epoxy and boron/epoxy gears. It is found that the reinforcement with kevlar/epoxy and carbon/epoxy is effec-

tive in improving the tooth strength, with kevlar/epoxy gears being the strongest. For the gears made of boron/epoxy, the critical section is mainly section 3, where the critical stress component is the transverse tensile stress.

A general trend observed is: Increasing the fiber volume ratios results in fiber failures in the direction normal to the fibers, i.e. fiber separation.

Acknowledgments

The authors would like to thank the CAD/CAM/Robotics Center of Middle East Technical University for providing computer facilities.

References

1. AGMA Standard 2001-B88, "Fundamental Rating Factors and Calculation Methods for Involute Spur and Helical Gear Teeth," 1988.
2. Alagöz, Ç. *Finite Element Analysis of Long Fiber Reinforced Composite Spur Gears*, M.Sc. Thesis, 1999, Mechanical Engineering Department, Middle East Technical University, Ankara, Turkey.
3. Arikan, M.A.S. *Computer Aided Dynamic Modelling of Spur Gears*, Ph.D. Thesis, 1987, Mechanical Engineering Department, Middle East Technical University, Ankara, Turkey.
4. Arikan, M.A.S. "Determination of Maximum Possible Contact Ratios for Spur Gear Drives with Small Number of Teeth," *Proceedings of 1995 ASME Design Engineering Technical Conferences*, 1995, DE-Vol. 82, pp. 569–576.
5. Herakovich, C.T. *Mechanics of Fibrous Composites*, John Wiley & Sons, New York, 1998.
6. Lo, S.H. "A New Mesh Generation Scheme For Arbitrary Planar Domains," *International Journal for Numerical Methods in Engineering*, 1985, Vol. 21, pp. 1403–1426.
7. Oda, S., K. Nagamura and K. Aoki. "Stress analysis of Thin Rim Spur Gears by Finite Element Method," *Bulletin of the JSME*, 1981, Vol. 25, p. 1273.
8. Shiratori, E., et al. "A Study of Molding Method and Static Strength of Carbon Fiber-Reinforced Plastic Gear," *Bulletin of the JSME*, 1986, Vol. 24, No. 198, pp. 2177–2183.
9. Tanaka, S. and K. Morimoto. "Accuracy and Wear Resistance of Small Injection-Molded Plastic Gears Filled with Fiber or Carbon," *JSME International Journal*, 1991, Vol. 34, No. 2, pp. 310–314.
10. Tsai, S.W. and H.T. Hahn. *Introduction to the Composite Materials*, Technomic Publishing Co., Lanchester, PA, 1980.
11. Tsukomato, N. and K. Teresima. "Fundamental Characteristics of Plastic Gears Made of Thermoplastic Resin Filled with Various Fibers," *JSME International Journal*, 1990, Vol. 33, No. 4, pp. 590–596.
12. Yixin, M. and F. Mingwu. "Advanced Two Dimensional Automatic Triangular Mesh Generation for

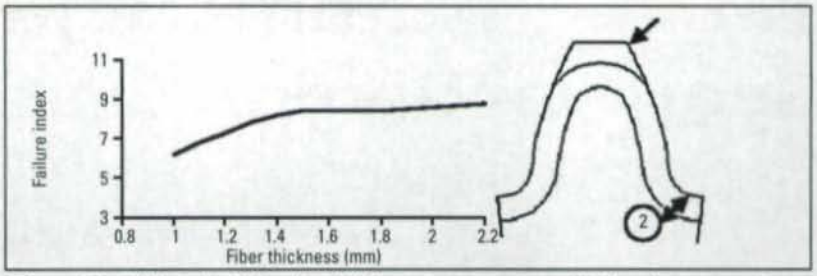

Figure 22—Effect of reinforcing thickness on gear strength (glass/epoxy gear).

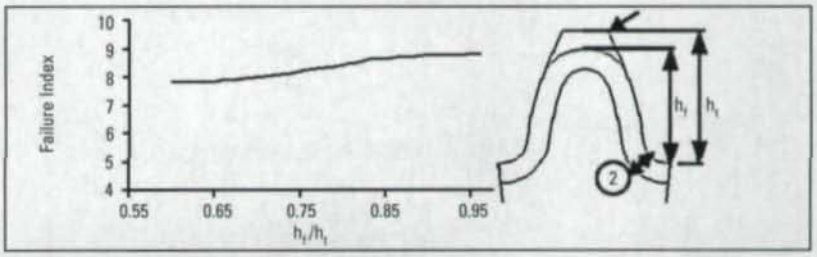

Figure 23—Effect of insertion depth on gear strength (glass/epoxy gear).

Table 9—Minimum Failure Indexes and Critical Sections for S-Glass/Epoxy Gear.

		V_{cf}			
		0.1	0.3	0.5	0.7
V_{lf}	0.1	3.90, 1*	4.58, 1	4.85, 1	4.95, 1
	0.3	4.63, 1	4.89, 1	4.68, 1	4.19, 1
	0.5	3.40, 2	3.99, 3	3.80, 3	3.27, 3

*(Minimum Failure Index: 3.90, Critical Section: 1)

Table 10—Minimum Failure Indexes and Critical Sections for Carbon/Epoxy Gear.

		V_{cf}			
		0.1	0.3	0.5	0.7
V_{lf}	0.1	5.99, 1	5.79, 2	5.85, 2	5.93, 2
	0.3	6.53, 1	6.10, 2	4.71, 2	4.73, 2
	0.5	5.97, 2	4.63, 3	4.55, 3	4.47, 3

Table 11—Minimum Failure Indexes and Critical Sections for Kevlar/Epoxy Gear.

		V_{cf}			
		0.1	0.3	0.5	0.7
V_{lf}	0.1	5.20, 1	5.99, 1	5.98, 3	5.83, 3
	0.3	6.31, 1	6.26, 1	5.99, 3	5.85, 3
	0.5	7.52, 1	6.44, 3	6.11, 3	6.02, 3

Table 12—Minimum Failure Indexes and Critical Sections for Boron/Epoxy Gear.

		V_{cf}			
		0.1	0.3	0.5	0.7
V_{lf}	0.1	5.10, 3	4.90, 3	4.40, 3	4.10, 3
	0.3	4.32, 3	3.94, 3	3.50, 3	3.94, 3
	0.5	3.80, 3	3.62, 3	3.20, 3	3.10, 3

Table 13—Fiber Volume Ratio Combinations which Result in the Weakest Gears.

	S-Glass/Epoxy	Carbon/Epoxy	Kevlar/Epoxy	Boron/Epoxy
V_{lf}	0.5	0.5	0.1	0.5
V_{cf}	0.7	0.7	0.1	0.7
Failure Index	3.27	4.47	5.20	3.10
Critical Section	3	3	1	3

Table 14—Fiber Volume Ratio Combinations which Result in the Strongest Gears.

	S-Glass/Epoxy	Carbon/Epoxy	Kevlar/Epoxy	Boron/Epoxy
V_{lf}	0.1	0.3	0.5	0.1
V_{cf}	0.7	0.1	0.1	0.3
Failure Index	4.95	6.53	7.52	4.90
Critical Section	1	1	1	3